RSC Advances

ROYAL SOCIETY OF CHEMISTRY

www.rsc.org/advances

A coral-inspired nanoscale design of Sn-Cu/PANi/GO hybrid anode materials for high performance lithium-ion battery

Peng Dou, [a] Anni Jiang, [a] Xin Fan, [a] Daqian Ma, [a] Xinhua Xu *[ab]

a School of Materials Science and Engineering, Tianjin University, Tianjin 300072, P. R. China. E-mail:xhxu_tju@eyou.com; Tel:+86-22-2740627. Fax: +86-22-2740627
b Tianjin Key Laboratory of Composite and Functional Materials, Tianjin 300072, P. R. China

Abstract

A facile and scalable synthesis approach is developed for fabrication of a three-dimensional (3D) polyaniline (PANi)/graphene oxide (GO) hybrid hydrogel evenly embed with hollow Sn-Cu nanoparticles (Sn-Cu NPs) as high performance anode for lithium-ion batteries. The hierarchical conductive hydrogel was prepared via in situ polymerization of aniline monomer on the surface of Sn-Cu NPs and GO nanosheets. The morphology and structure of the resulting hybrid materials have been characterized using scanning electron microscopy (SEM) and transmission electron microscopy (TEM). The hierarchical conductive hydrogel framework with dendritic PANi nanofibers and 2D GO nanosheets serve as a continuous 3D electron transport network and high porosity to accommodate the volume expansion of Sn-Cu NPs. The PANi coating plays an "artificial SEI" function to preserve the structural and interfacial stabilization of Sn-Cu NPs during the cycling processes. As a consequence of this 3D hybrid anode, an extremely long stable cycling performance is achieved with reversible discharge capacity over 693 mAh/g after 200 cycles at current rate of 0.2 C and a reversible capacity of 371 mAh/g retention at a much higher current rate of 2 C, suggesting that this novel Sn-Cu/PANi/GO composite is a promising candidate for energy storage applications.

1. Introduction

The requirement in developing rechargeable lithium-ion batteries with high energy density, long cycle life, and low cost has been increasing to satisfy the urgent needs for portable electronics, electric vehicles and grid-scale energy storage systems[1, 2]. However, the most widely used traditional anode material in lithium-ion batteries, graphite, does not meet with high energy needs due to its limited theoretical specific capacity of only about 372 mAh/g, and alternative anode materials with higher reversible and rate capacities as well as long-term cyclic stability are highly desired[3, 4]. In recent years, among the various anode candidates, Tin (Sn) has attracted a great deal of attention as one of the most promising anode materials for Li-ion batteries, primarily due to its exceptionally high specific capacity (994 mAh/g for $Li_{22}Sn_5$) and moderate operating voltage[5-7]. However, the development of this high-capacity anode material has been met with three significant challenges: high initial capacity loss, poor capacity retention in prolonged cycling, and low rate capability[8]. High initial capacity

loss is caused by irreversible secondary reaction such as the formation of a solid electrolyte interphase (SEI) [4-7, 11, 12]. Previous research has clearly indicated that the interface between the electrode active material and the electrolyte is crucial to the electrochemical performance of lithium ion battery[9, 10]. Poor capacity retention and low rate capability is generally attributed to the dramatic volume change during insertion and extraction of lithium ion, which results in not only severe pulverization and subsequent electrical disconnection from the current collector, but also an unstable SEI growth on the Sn surfaces upon cycling[11, 12].

To circumvent these issues, most of the research has focused on the development of various nanostructures of Sn-based materials, including nanoparticles[7, 11-13], nanorods[14], hollow spheres[15, 16], and Sn/carbon nanocomposites[17-19]. Among them, hollow nanostructures is presently studied as a major approach for mitigating the effects of the volume changes and to enhance the reaction kinetics on the basis of the following consideration[20, 21]: 1) the larger surface area of the hollow structures enable better access for lithium ion as results of the increased electrode-electrolyte contact area and the significantly reduced diffusion paths. The shorter diffusion paths lead to a better rate capability, and the overall capacity is higher as a result of the larger number lithium-storage sites. 2) The hollow interior provides additional free volume to alleviate the structural strain associated with repeated Li^+ insertion/extraction processes and thus leads to improved cycling stability.

Recently, a substantial amount of research has involved modifying the properties of the interface between the electrode active material and the electrolyte to improve the overall performance of lithium-ion battery anodes[22]. A commonly adopted approach is to precondition the surfaces of active materials with coatings. Surface coating can confine the volume change and change the reaction chemistry of SEI formation during battery operation. The coating becomes part of the SEI; therefore, the coating has sometimes been referred to as an "artificial SEI"[23]. The majority of artificial SEI research has used inorganic oxide, carbon or polymer coatings. The inorganic oxide and carbon coating features advantages of favorable chemical and structural stabilities but exhibits disadvantages of limited flexibility to compensate the large volume change and high processing temperatures. By contrast, polymer (especially conducting polymer) as a unique class of coating possesses excellent advantages[24]. The soft polymer matrix can not only avoid the direct exposure of encapsulated nanoparticles to the electrolyte and preserve the interfacial stabilization between electrode and electrolyte, but also suppress the aggregation of nanoparticles and buffer the volume expansion. Typically，single component of conducting polymers, such as polyaniline, polypyrrole, and poly(3,4-ethylenedioxythiophene), have been explored as artificial SEI and demonstrated to effectively buffer the substantial volume change, and offer electrical conduction pathways to the active materials, leading to considerably improved cycle stability and a higher reversible specific capacity[25-27]. Nevertheless, research on shape control of conducting polymer coatings is limited. The advantage of conducting polymer has yet to be fully explored for greater impact on the lithium ion batteries.

Generally, electrodes made from nanoparticles require using polymer binder and

conductive additive. In order to increase mass loading of the active materials on the current collector without sluggish Li^+ intercalation, 3D porous nanostructured conductive binder was better to help improve battery electrochemical performance than bulk[28, 29]. In recently, conducting polymer hydrogels (CPHs) have been attracting increasing attention because of their large specific surface areas, high conductivities, good electrochemical activity and biocompatibility[30]. In addition, CPHs also provide excellent processability, they can be easily cast into thin films or be ink-jet printed into micropatterns[31]. Using it as a novel electronically conductive binder for silicon anode has been demonstrated can effectively improve the transport of both electrons and ions, and long-term cycling stability [28, 29, 32]. However, the electrical conductivity and mechanical strength of these conductive binders are still need to be improved.

Herein, inspiring by the previous works, we put forward a novel and scalable in-situ polymerization of PANi/GO hybrid hydrogel to anchor Sn-Cu NPs as high performance lithium-ion battery anode. In this constructed Coralline architecture, the elastic hydrogel consists of a hierarchical 3D porous network that composes of dendritic PANi nanofibers and GO nanosheets. The GO nanosheets act as robust connector to preserve structural integrity and enhance electronic conductivity of the hydrogel. Hollow Sn-Cu NPs can reduce internal strain and shorten lithium diffusion length to improve electrochemical performance of Sn-based materials. The PANi coating can effectively not only preserve the structural and interfacial stabilization but also avoid the aggregation and buffer the volume expansion of Sn-Cu NPs, while also serve as a continuous 3D pathway for electronic conduction. As a consequence of this 3D hybrid anode, outstanding electrochemical performance has been achieved, such as stable and high reversible capacity, high coulomb efficiency, and superior rate capacities upon increased currents. Furthermore, the all solution based process represents a potentially scalable preparation method toward practical industrial manufacturing.

2. Experimental

2.1. Materials

Stannous sulfate ($SnSO_4$, >99%), poly(vinylpyrrolidone) (PVP), sodium borohydride ($NaBH_4$, >98%), sodium hydroxide (NaOH, >96%), sodium dodecyl sulfate (SDS), cupric chloride ($CuCl_2 \cdot 2H_2O$), Ethanol (>99%), sodium nitrate, concentrated sulfuric acid (>98%), potassium permanganate, ammonium persulfate (APS) were obtained from Kewei Chemical Reagent Co. Ltd. Tianjin University (Tianjin, China). Aniline monomer (98% reagent grade) and phytic acid (60% w/w in H_2O) were purchased from Sigma Aldrich PTE. Ltd. All reagents were used as received except aniline which was distilled prior to use.

2.2. Preparation of GO Nanosheets

GO nanosheets were prepared from commercially available graphite by a modified Hummers method[33, 34]. 2 g of natural flake graphite and 2 g of sodium nitrate were mixed in a 500 mL round-bottomed flask. Concentrated sulfuric acid was then added to the mixture under ice-bath cooling. During the following stages the mixture was continuously stirred using a magnet stirrer. 12 g of potassium permanganate was

slowly added to the solution mixture while keeping the temperature at 0 °C. After stirring for 90 min, the whole pot was transferred to a warm water bath (35 °C) for 2 h. 80 mL of deionized (DI) water was slowly dropped into the solution and left stirring for another 30 min, after which it was further diluted by 200 mL of deionized water. Following the dilution, 12 mL of hydrogen peroxide was added dropwise into the solution. The solution was filtered and washed until the filtrate became pH neutral. Then, GO was subjected to dialysis for 7 days to completely remove metal ions and acids. Then, the solution after dialysis was sonicated for 2 h, and afterward, a brown homogeneous supernatant was collected.

2.3. Synthesis of PANi hydrogel

PANi hydrogel was synthesized according to the following solution processes. First, solution A was prepared by dissolving 0.3 mmol aniline monomer and 0.1 mmol phytic acid in 1 mL of deionized water while stirring. Second, 0.5 ml solution B, containing 0.3 mmol ammonium persulfate, was added into the solution A and subjected to ~1 min bath sonication. In about 2 min, the solution changed colour from brown to dark green and became viscous and gel-like, indicating polymerization of aniline monomer to form the PANi hydrogel.

2.4. Preparation of Sn-Cu/PANi/GO hybrid hydrogel

The hollow Sn-Cu NPs were synthesized via galvanic replacement reaction in our previous works[15]. The ternary Sn-Cu/PANi/GO composite hydrogel was synthesized via a similar route of the synthesis of PANi hydrogel, except that GO and hollow Sn-Cu NPs were added into solution A. Typically, GO was dissolved in 1 mL DI water, 80 mg Sn-Cu NPs were dispersed in it, 0.3 mmol aniline monomer and 0.1 mmol phytic acid was added into the solution while stirring to form solution A. Solution B was prepared by dissolving 0.3 mmol ammonium persulfate in 0.5 mL DI water. The A and B solutions were cooled to 4 °C and then mixed quickly. In about 3 min, the solution changed colour from gray to dark green and became viscous and gel-like, indicating to form the composite hydrogels. In the end, Sn-Cu/PANi/GO composite hydrogels were collected after removing excessive phytic acid through extensive rinsing with DI water.

2.5. Characterization

The morphology and structure of the as-prepared samples were investigated by a Hitachi S-4800 field-emission scanning electron microscope (FE-SEM) at an accelerating voltage of 5 kV and a high resolution transmission electron microscope (HR-TEM, JEM-2100F) operated at 200 kV. FTIR were recorded on a NEXUS 870 spectrophotometer.

In order to measure the electrochemical performance, Sn-Cu/PANi/GO composite electrodes were prepared by coating the viscous Sn-Cu/PANi/GO hydrogels onto a Cu foil current collector (no binder used) and drying in vacuum at room temperature. The coin-type half-cells fabricated in an argon-filled glovebox, contained the working electrode, a Li metal foil counter/reference electrode, and a microporous separator soaked in electrolyte. The electrolyte solution is 1.0 M LiPF6 in 1:1 w/w ethylene carbonate/diethyl carbonate. Electrochemical impedance spectroscopy measurement was carried out on Parstat 2263 Electrochemical workstation system. Galvanostatic

cycling was done using an LAND 8 Channels battery tester in the potential range of 0.01-2.0 V. The specific capacity was calculated based on the mass of Sn-Cu NPs. The charge/discharge rate was calculated assuming the theoretical capacity of Sn (994 mAh/g). The coulombic efficiency was calculated as Cdealloy/Calloy, where Cdealloy and Calloy are the capacity of the anodes during Li extraction and insertion.

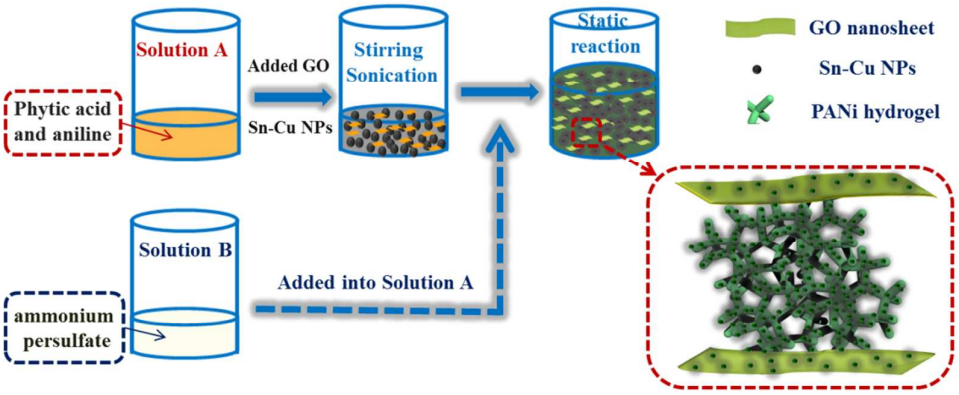

Fig. 1 Schematic illustration of the fabrication of 3D Sn-Cu/PANi/GO ternary hydrogel. Phytic acid plays the role as a dopant and a crosslinker. The GO nanosheets act both as the wrapping layer and conductive backbone, which further enhance the integration of Sn-Cu NPs/PANi framework and electric conductivity of the electrode. Sn-Cu NPs are encapsulated within thin PANi coating layer and closely incorporated within the conductive framework.

3. Results and discussion

The overall synthetic procedure and the detailed structure of 3D Sn-Cu/PANi/GO ternary hydrogel were schematically illustrated in fig. 1. To achieve the 3D hydrogel, aniline, which serve as the monomer, and phytic acid, which serve as both the crosslinker and dopant, were first added into the solution A. Then the as-prepared solution A was mixed with Sn-Cu NPs and GO to form gray slurry. Phytic acid react with PANi by protonating the imine groups on PANi, and each phytic acid molecule can interact with more than one PANi chain, this crosslinking effect not only results in the formation of connected PANi network fix with in situ coated Sn-Cu NPs, but also further improve the conductivity of the PANi hydrogel through protonic acid doping. Afterward, solution B containing the oxidative initiator was added into it to form viscous dark green Sn-Cu/PANi/GO ternary hydrogel. The novel 3D conductive framework is constructed by the nanostructured PANi hydrogel, offering both nanoscale pores to facilitate the penetration of electrolyte ions and micrometer sized pores to accommodate the Sn-Cu NPs and their volume changes in the charge/discharge processes. Simultaneously, a thin in situ polymeric layer was coated on the surface of Sn-Cu NPs and GO nanosheets, which provided the electrical connections and preserved the structural stabilization and suppressed the aggregation of Sn-Cu NPs to further improve the electrochemical performance. Since part of the Sn-Cu NPs may detach from the current collector after a number of cycles due to the volume expansion, the interlaced GO and PANi framework could still maintain the

electrical connection within the entire electrode[35].

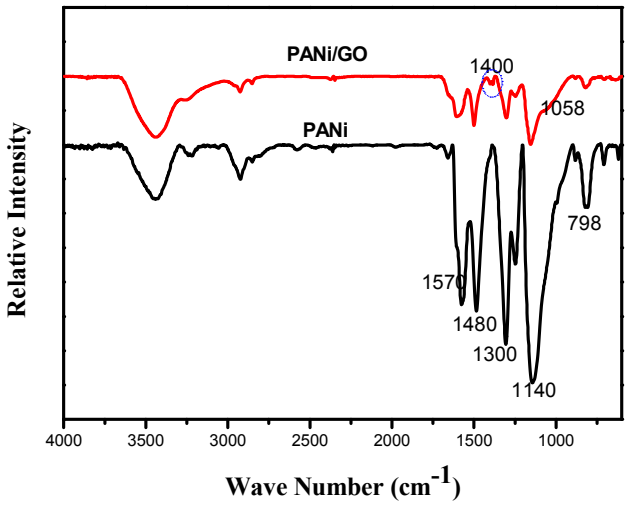

Fig. 2 FTIR spectra of PANi and PANi/GO hydrogels

It is well known that the physical structure and chemical composition of coating layer exert profound effects on various aspects of the electrode performance[23]. Thus, an FTIR spectroscopy analysis was first employed to reveal the chemical structure of PANi and PANi/GO hydrogels. The chemical structure of the as-synthesized composite hydrogel was presented in Fig. 2. The characteristic peaks at 1570 and 1480 cm^{-1} are due to the stretching vibration of quinoid ring and benzenoid ring, respectively, which indicates that the chemical structure of phytic acid doped PANi are emeraldine rather than solely leucoemeraldine or permigraniline form. The absorption peaks at 1300 and 1246 cm^{-1} were attributed to the C-N stretching vibration with aromatic conjugation. The bands at 789 and 505 cm^{-1} can be assigned to the bending vibrations of the C-H bonds within the 1,4-disubstituted aromatic ring. The peaks at 1400, 1220 and 1058 cm^{-1} were attributed to carboxy, epoxy, and alkoxy groups situated at the edges of the GO nanosheets were also found, as reported elsewhere[36]. Furthermore, the FTIR results clearly show that the aromatic ring of PANi enables π-π attractive interaction with the GO surface to achieve strong adhesion. This feature can effectively preserve structural integrity and enhance electronic conductivity of the hydrogel.

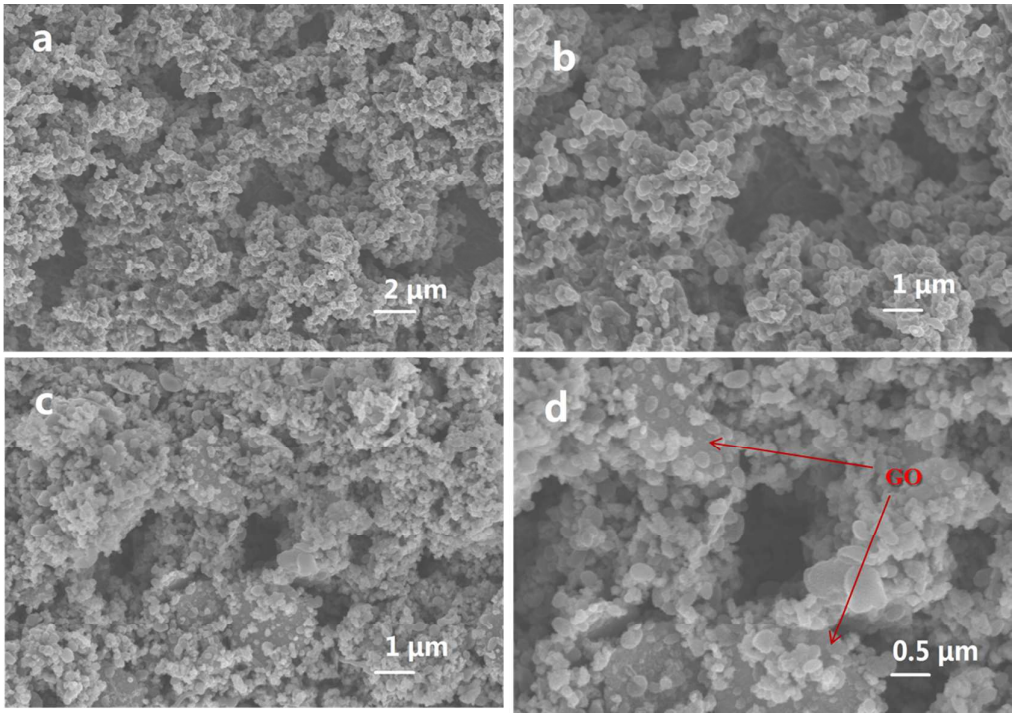

Fig. 3 Morphology and microstructure of 3D Sn/PANi/GO hydrogel. (a, b) SEM images of a Sn-Cu/PANi composite electrode at low and high magnifications. (c, d) SEM images of a Sn-Cu/PANi/GO hierarchical nanostructured electrode. The red arrows indicate GO nanosheets.

The detailed morphology and structure information of the Sn-Cu/PANi/GO hydrogel electrode was illustrated by SEM and TEM. Typically, SEM image (Fig. 3a, b) demonstrated the hierarchically porous nanostructures of the Sn-Cu/PANi hydrogel composite electrode. Further investigation by TEM revealed that the PANi forms a continuous network (Fig. 4c). The conducting hydrogel consists of a hierarchical 3D porous network which be composed of PANi dendritic nanofibers and 2D GO nanosheets. The GO interlaced on and across the Sn-Cu/PANi bulk. The formed PANi/GO network could increase electronic conductivity of the electrode, while the nanoscale and the micrometer-sized pores can facilitate liquid electrolyte diffusion into the electrode and offer free space to spatially accommodate the volume expansion of the Sn-Cu NPs during electrochemical cycling. The in-situ formed PANi layer on the Sn-Cu NPs surface was ~10nm thick (fig. 4d), which avoid the direct exposure of Sn-Cu NPs to the electrolyte and preserve the interfacial stabilization between electrode and electrolyte, which is beneficial for achieving high rate and excellent cycling stability performance[23, 37].

Fig. 4a and b show the TEM and HRTEM images of mono-dispersed hollow Sn-Cu NPs, their diameter is in the range of 10-20 nm, and the thickness of shell is about 5 nm. This hollow structure has higher surface area, shorter path length for Li^+ transport, and more space to buffer the volume change during lithium insertion and extraction[38]. HRTEM image of 3D Sn-Cu/PANi/GO hydrogel revealed that the polymeric coating on Sn-Cu NPs was uniform and connected as present in Fig. 4d. The conductive PANi

layers can effectively avoid the aggregation and buffer the volume expansion of Sn-Cu NPs, while also serves as a continuous 3D electronic pathway for the superior electrochemical performance of the Sn-Cu/PANi/GO hydrogel. Simultaneously, the PANi coating acts as artificial SEI help better improve the structural and interfacial stabilization.

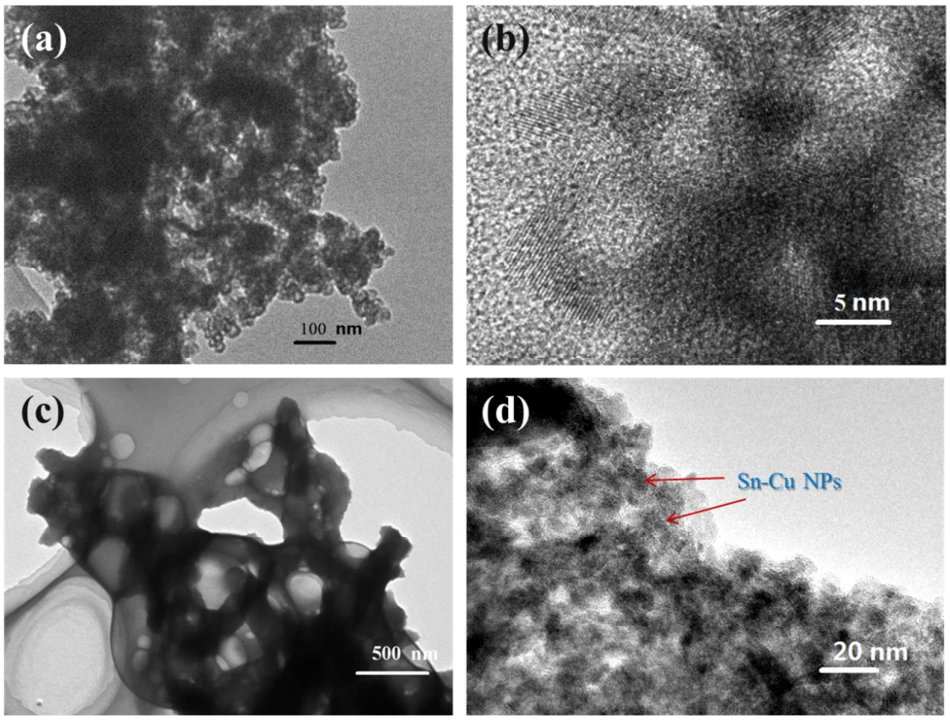

Fig. 4 (a, b) TEM and HRTEM images of hollow Sn-Cu NPs. (c) TEM image of PANi/GO hydrogel. (d) HRTEM image of 3D Sn-Cu/PANi/GO hydrogel.

The unique morphology and structure of the as-prepared 3D Sn-Cu/PANi/GO composite motivated us to further investigate its electrode performance. The electrochemical cycling performance of the composite electrode was evaluated using galvanostatic charge–discharge cycling from 2.0 to 0.01 V as shown in Fig. 5a and b. The 3D Sn-Cu/PANi/GO hydrogel electrode exhibited excellent electrochemical characteristics. Fig. 5a shows the potential profiles result at a rate of 0.2 C. Unlike the voltage profile of pure Sn electrode, the Sn-Cu/PANi/GO electrode has relatively smooth voltage profile due to the multi-step Li-Sn alloy reactions of Sn and Cu_6Sn_5[15], and PANi coating layer may influence the overall change in phase-change rate 39. The voltage region below 0.7 V in the cathodic process corresponds to the multi-step the conversion of crystalline Sn-Cu to Li_xSn alloy phase ($Sn+xLi^+ + xe^- = Li_xSn$); the potential plateau around 1.2 V at the first few times corresponds to irreversible reaction and the formation of SEI layer[40]. The first discharge/charge cycle delivers a specific charge capacity of 1259 mAh/g and a discharge capacity of 1466 mAh/g, corresponding to a Coulombic efficiency of 85%. This initial capacity loss can be attributed to the SEI formation on the surface of electrode and the decomposition of electrolyte during the first charge/discharge step[39, 41]. It is important to note that both

charge and discharge profiles exhibited little change from the thirtieth to 200th cycles, demonstrating that the 3D Sn-Cu/PANi/GO electrode are very stable during cycling. The greatly improved cycling performance and life-span of the electrode could be attributed to Sn-Cu NPs well confined within the 3D conductive framework. The in-situ formed PANi coating layer can help to form stable SEI[28, 29]. Fig. 6b shows the SEM image of the Sn-Cu/PANi/GO electrode after 200 electrochemical cycles after the removal of SEI layer. The intrinsic 3D porous structure remained barely changed after 200 cycles. The Sn-Cu NPs are still confined inside the hydrogels owing to the in situ formed polymeric layer on the surface of Sn-Cu NPs as well as the GO nanosheets.

To further highlight the superiority of the 3D Sn-Cu/PANi/GO composite as anode material of lithium-ion battery, the Sn-Cu NPs and Sn-Cu/PANi electrodes were also investigated under the same conditions. Fig. 5c exhibits cycle performances of these three electrodes at a current density of 0.2 C. As can be seen, the Sn-Cu/PANi/GO electrode shows superior cycling performance. In contrast, a much lower reversible capacity (~526 mAh/g) of the Sn-Cu/PANi composite is delivered at the end of the 100 cycles. As for the pure Sn-Cu NPs, they exhibit very fast capacity fading and have a low reversible capacity of ~310 mAh/g after the 100th cycle. This could be attributed to serious partial pulverization induced the repeated formation of SEI film and peeled off from the current collector[16]. Therefore, the Sn-Cu/PANi/GO electrode was demonstrated have remarkably higher reversible capacity and cycling stability, which are ascribed largely to the strong synergistic effect between the conductive 3D network hydrogel and PANi coating layer of Sn-Cu NPs. During the cycle process, the PANi coating layer and GO nanosheets around Sn-Cu NPs is very beneficial for the growth of a stable SEI film and thus can prevent the rupture of the SEI during cycling, leading to excellent cycling stability. In addition, the coating layer can restrain the agglomeration of Sn-Cu NPs to large particles, which is also very help for enhancing the cycling stability.

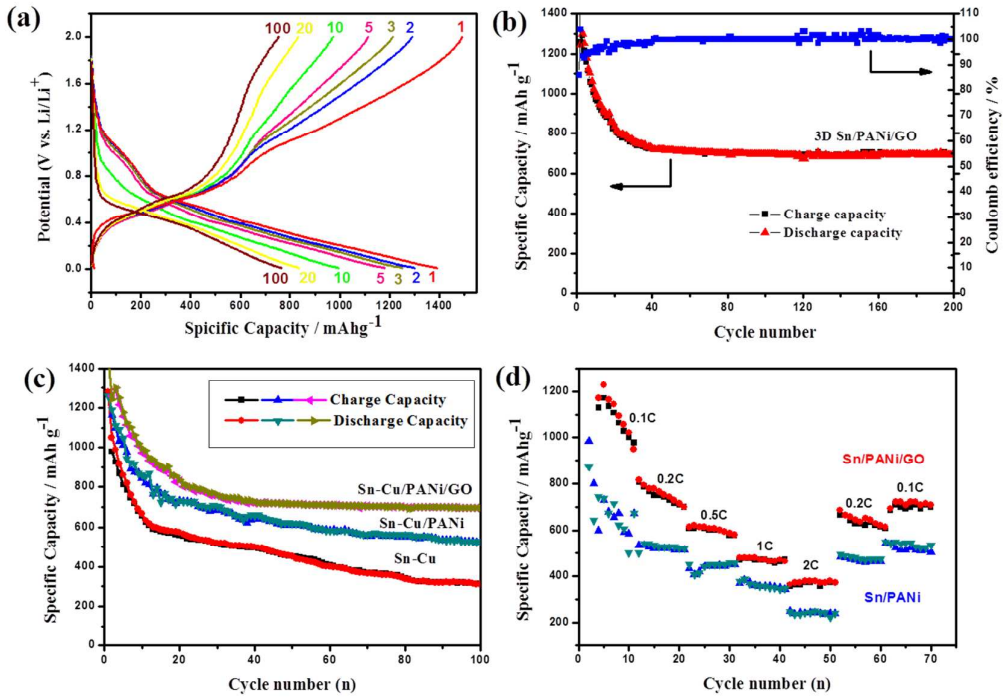

Fig. 5 (a) Voltage profiles of the Sn-Cu/PANi/GO electrode at a current density of 0.2 C. (b) Cycle performance and Coulombic efficiency of the Sn-Cu/PANi/GO electrode at current density of 0.2 C for the 200 cycles. (c) Cycle performance of the Sn-Cu/PANi/GO, Sn-Cu/PANi, and Sn-Cu NPs electrodes at a current density of 0.2 C. (d) Rate cycle performance of the electrodes of Sn-Cu/PANi/GO and Sn-Cu/PANi at charge/discharge rates from 0.1 to 2 C (1 C= 1 A/g) for 70 cycles.

For practical applications, the composite electrode needs to be examined over a wide range of operating rates. Fig. 5d shows the corresponding rate capability with the various rates stepwise increased from 0.1 C to 2 C and then switched back. In the first rate cycle of the 3D Sn-Cu/PANi/GO composite electrode, the average reversible capacities are 1135, 750, 607, 471, and 364 mAh/g at the increasing current densities of 0.1, 0.2, 0.5, 1, and 2 C, respectively. When the current densities decrease back from 2 C to 0.2, and 0.1 C, the reversible capacities recover from 364 mAh/g to 628, and 707 mAh/g. Although the rate of 2 C was imposed on this electrode, its corresponding specific capacities were still as high as 364 mAh/g. All of these values are more than the theoretical specific capacity of the commonly used graphite anode material. The stability to maintain a large capacity at various high rates for the composited anodes can be attributed to the highly conducting 3D electronic conductive network, the shorter lithium diffusion length from the porous nanostructure, large electrode/electrolyte contact area and better accommodation for volume change during the charging/discharging process[28].

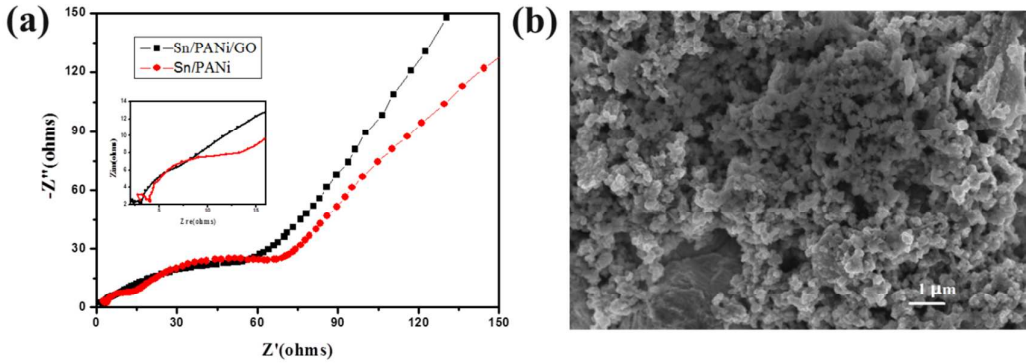

Fig. 6 (a) Nyquist plots of Sn-Cu/PANi/GO and Sn-Cu/PANi at fresh coin cells over the frequency range from 1 MHz to 0.01 Hz. (b) Typical SEM image of a 3D Sn-Cu/PANi/GO hybrid electrode after 200 electrochemical cycles.

In order to understand the reasons for the much higher rate performance of the 3D Sn-Cu/PANi/GO composite than that of the Sn-Cu/PANi composite, the impedances of the 3D Sn-Cu/PANi/GO and Sn-Cu/PANi composite at fresh coin cells were investigated using electrochemical impedance spectroscopy (EIS), and the results are displayed in fig. 6a. As can be seen, both the impedance spectra have similar features. The semicircle at high frequency region is an indication of SEI resistance (R_{SEI}) and contact resistance (R_f), the medium frequency region reflects the charge transfer resistance (R_{ct}) on the interface between electrode and electrolyte, and the straight line in low frequency region provides information on the diffusion of lithium ion in the electrode (R_e). The smaller semicircle signifies a smaller resistance, and the larger slop of the straight line represents that is more beneficial to the conductivity of lithium ions[23, 42-43]. According to fig. 6a, it can be found clearly that the diameter of the semicircle for the Sn-Cu/PANi/GO electrode in the high frequency region is significantly smaller than that of the Sn-Cu/PANi electrode, which implies that the GO and 3D porous structure could effectively enhance the electrical conductivity and reduce the contact and charge transfer resistances in the electrode, which contributing to the remarkable improvements on the reversible capacity and rate capability.

4. Conclusions

In summary, a unique coral like 3D Sn-Cu/PANi/GO nanostructured electrode was fabricated by a facile and scalable solution process. By taking advantage of the conductive polymer matrix, which provides fast electronic and ionic transfer channels, as well as free space for Sn-Cu NPs volume changes, outstanding electrochemical performance has been achieved. The PANi coating layer and GO nanosheet around Sn-Cu NPs is very beneficial for the growth of a stable SEI film and thus can prevent the rupture of the SEI during cycling, leading to excellent cycling stability. As a result, compared to the pure Sn-Cu NPs, we successfully achieved high capacity and extremely stable electrochemical cycling. The composites can deliver a reversible specific capacity of ~693mAh/g even after 200 cycles at a charge/discharge rate of 0.2 C. Moreover, this promising material design and the concept of the facile synthesis

method are expected be useful for potential application in catalysis and sensors.

Acknowledgements

This work was financially supported by the National Natural Science Foundation of China (no. 51143009 and 51273145).

Notes and references

1 J. M. Tarascon and M. Armand, *Nature*, 2001, 414, 359.
2 M. Armand and J. M. Tarascon, *Nature*, 2008, 451, 652.
3 A. R. Kamali and D. J. Fray, *Rev Adv Mater Sci*., 2011, 27, 14.
4 J. Qin, C. N. He, N. Q. Zhao, Z. Y. Wang, C. S. Shi, E. Z. Liu and J. J. Li, *ACS Nano*, 2014, 8, 1728.
5 R. Z. Hua, M. Zhu, H. Wang, J. W. Liu, O. Liuzhang and J. Zou, *Acta Mater.*, 2012, 60, 4695.
6 K. V. Kravchyk, L. Protesescu, M. I. Bodnarchuk, F. Krumeich, M. Yarema, M. Walter, Ch. Guntlin and M. V. Kovalenko, *J. Am. Chem. Soc.*, 2013, 135, 4199.
7 L. P. Xu, C. Kim, A. K. Shukla, A. Dong, T. M. Mattox, D. J. Milliron and J. Cabana, *Nano Lett*., 2013, 13, 1800.
8 Z. Q. Zhu, S. W. Wang, J. Du, Q. Jin, T. R. Zhang, F. Y. Cheng and J. Chen, *Nano Lett.*, 2014, *14*, 153.
9 L. J. Fu, H. Liu, C. Li, Y. P. Wu, E. Rahm, R. Holze, H. Q. Wu, *Solid State Sci.*, 2006, 8, 113.
10 P. Verma, T. Sasaki, P. Novak, *Electrochim. Acta*, 2012, 82, 233.
11 M. G. Kim, S.J. Sim and J. Cho, *Adv Mater*., 2010, 22, 5154.
12 B. Wang, B. Luo, X. L. Li and L. J. Zhi, *Mater Today*, 2012, 15, 545.
13 H. K. Zhang, H. H. Song, X. H. Chen, J. S. Zhou, *J. Phys. Chem. C,* 2012, 116, 22774.
14 D. H. Nam, T. H. Kim, K. S. Hong and H. S. Kwon, *ACS Nano*, 2014, 8, 11824.
15 X. Fan, X. N. Tang, D. Q. Ma, P. Bi, A. N. Jiang, J. Zhu and X. H. Xu, *J. Solid State Electrochem.*, 2014, 18, 1137.
16 H. S. Hou, X. N. Tang, M. Q. Guo, Y. Q. Shi, P. Dou and X. H. Xu, *Mater Lett.*, 2014, 128, 408.
17 S. D. Seo, G. H. Lee, A. H. Lim, K. M. Min, J. C. Kim, H. W. Shim, K. S. Park and D. W. Kim, *RSC Adv.*, 2012, 2, 3315.
18 S. R. Gowda, A. L. M. Reddy, M. M. Shaijumon, X. B. Zhan, L. J. Ci, P. M. Ajayan, *Nano Lett*, 2011, 11, 101
19 W. B. Yue, S. Yang, Y. Ren and X. J. Yang, *Electrochim. Acta*, 2013, 92, 412.
20 X. Lai, J. E. Halpert, D. Wang, *Energy Environ. Sci.,* 2012, 5, 5604.
21 J. Y. Wang, N. L. Yang, H. J. Tang, Z. H. Dong, Q. Jin, M. Yang, D. Kisailus, H. J. Zhao, Z. Y. Tang and D. Wang, *Angew. Chem. Int. Ed*. 2013, 52, 6417.
22 E. Kramer, R. Schmitz, P. Niehoff, S. Passerini, M. Winter, *Electrochim. Acta,* 2012, 81, 161.

23 F. S. Li, Y. S. Wu, J. Chou, M. Winter and N. L. Wu, *Adv Mater*., 2015, 27, 130.
24 K. C. Hsu, C. E. Liu, P. C. Chen, C. Y. Lee, H. T. Chiu, *J. Mater. Chem.,* 2012, 22, 21533.
25 Z. F. Li, H. Y. Zhang, Q. Liu, Y. D. Liu, L. Stanciu and J. Xie, *ACS Appl. Mater. Interfaces*, 2014, 6, 5996.
26 F. Han, D. Li, W. C. Li, C. Lei, Q. Sun and A. H. Lu, *Adv. Funct. Mater.,* 2013, 23, 1692.
27 P. J. Zhang, L. B. Wang, J. Xie, L. W. Su and C. A. Ma, *J. Mater. Chem. A,* 2014, 2, 3776.
28 H. Wu, G. Yu, L. Pan, N. Liu, M. T. McDowell, Z. Bao and Y. Cui, *Nat. Commun.*, 2013, 4, 1.
29 B. R. Liu, P. Soares, C. Checkles, Y. Zhao and G. H. Yu, *Nano lett*., 2013, 13, 3414.
30 L. J. Pan, G. H. Yu, D. Y. Zhai, H. R. Leec, W. T. Zhao, N. Liu, H. L. Wang, B. C. K. Tee, Y. Shi, Y. Cui and Z. N. Bao, *PANS*, 2012, 109, 9287.
31 Y. Zhao, B. R. Liu, L. J. Pan and G. H. Yu, *Energ Environ Sci*., 2013, 6, 2856.
32 R. Temmer, R. Kiefer, A. Aabloo and T. Tamm, *J. Mater. Chem. A*, 2013, 1, 15216.
33 F. W. Yuan and H. Y. Tuan, *Chem. Mater.*, 2014, 26, 2172.
34 J. Q. Zhao, S. F. Pei, W. C. Ren, L. B. Gao and H. M. Cheng, *ACS NANO*, 2010, 4, 5245.
35 G. H. Yu, L. B .Hu, N. A. Liu, H. L. Wang, M. Vosgueritchian, Y. Yang, Y. Cui and Z. A. Bao, *Nano Lett.*, 2011, 11, 4438.
36 J. W. An, J. H. Liu, Y. C. Zhou, H. F. Zhao, Y. X. Ma, M. L. Li, M. Yu and S. M. Li, *J. phys. chem. C*, 2012, 116, 19699.
37 G. Q. M, Z. Y. Wen, J. Jin, Y. Lu, X. W. Wu, M. F. Wu and C. H. Chen, *J. Mater. Chem. A*, 2014, 2, 10350.
38 J. Liu and D. F. Xue, *Nanoscale Res Lett.*, 2010, 5, 1525.
39 M. J. Noh, Y. J. Kwon, H. J. Lee, J. P. Cho, Y. J. Kim and M. G. Kim, *Chem. Mater.*, 2005, 17, 1926.
40 W. Ni, J. L. Cheng, L. Y. Shi, X. D. Li, B. Wang, Q. Guan, L. Huang, G. F. Gu and H. Li, *J. Mater. Chem. A*, 2014, 2, 19122.
41 D. N. Wang, X. F. Li, J. L. Yang, J. J. Wang, D. S. Geng, R. Y. Li, M. Cai, T. K. Sham and X. L. Sun, Phys. Chem. *Chem. Phys.*, 2013, 15, 3535.
42 Y. S. Hu, R. Demir-Cakan, M. M. Titirici, J. O. Muller, R. Schlogl, M. Antonietti and Maier, *Angew. Chem. Int. Ed.*, 2008, 47, 1645.
43 Z. Q. Zhu, S. W. Wang, J. Du, Q. Jin, T. R. Zhang, F. Y. Cheng and J. Chen, *Nano Lett.*, 2014, 14, 153.